

Article

Sulfur Removal and Iron Extraction from Natrojarosite Residue of Laterite Nickel Ore Processing by Reduction Roasting

Zulfiadi Zulhan ^{1,*} , Zhahrina Adzana ¹, Mona Munawaroh ¹, Achmad Haerul Yusro ², Jonathan Dwiputra Christian ¹, Aura Dwi Saputri ¹ and Taufiq Hidayat ¹

¹ Metallurgical Engineering Department, Faculty of Mining and Petroleum Engineering, Institut Teknologi Bandung, Jl. Ganesa No. 10, Bandung 40132, Indonesia

² PT. Hydrotech Metal Indonesia, Jl. Raya Narogong km 26, Klapanunggal, Bogor 16710, Indonesia

* Correspondence: zulfiadi.zulhan@itb.ac.id

Abstract: An alternative laterite nickel ore processing using sulfuric acid as a leaching agent to produce class 1 nickel as a raw material for electric vehicle batteries produces natrojarosite residue as a by-product during the precipitation of iron and aluminum step. The natrojarosite residue contained iron and high sulfur, which is challenging to utilize as an iron source for steel manufacturing since sulfur can contaminate the steel product. This study focuses on sulfur elimination and iron extraction from natrojarosite. The natrojarosite was roasted for sulfur removal isothermally at different temperatures ranging from 500 until 1100 °C for 4 h. Roasting at 1100 °C resulted a decrease in sulfur content from 12.18% to 3.81% and an increase in iron content from 16.23% to 28.54%. The sulfur released during roasting can, in principle, be recirculated to a sulfuric acid plant and reused as a leaching agent in the nickel ore processing plant. The unroasted and roasted natrojarosite residues were then reduced by coconut shell charcoal in the temperature range of 1000–1400 °C. The results showed that the metallic iron could be obtained from both unroasted and roasted natrojarosite residue at a temperature of 1200 °C and higher. The sulfur content in the oxide phase of unroasted natrojarosite residue was significantly higher than roasted natrojarosite residue. However, the roasting did not significantly influence the sulfur content in the metal phase. The sulfur content in the metal phase from unroasted and roasted natrojarosite residue was less than 1.2%. This result indicated that the removal of sulfur and metal oxide reduction in the natrojarosite residue could be carried out simultaneously in one stage where the natrojarosite residue is reduced by carbonaceous material at a temperature of 1200 °C or higher.

Keywords: laterite nickel; natrojarosite residue; sulfur removal; metal extraction



Citation: Zulhan, Z.; Adzana, Z.; Munawaroh, M.; Yusro, A.H.; Christian, J.D.; Saputri, A.D.; Hidayat, T. Sulfur Removal and Iron Extraction from Natrojarosite Residue of Laterite Nickel Ore Processing by Reduction Roasting. *Metals* **2023**, *13*, 52. <https://doi.org/10.3390/met13010052>

Academic Editor: Chenguang Bai

Received: 30 October 2022

Revised: 20 November 2022

Accepted: 20 December 2022

Published: 24 December 2022



Copyright: © 2022 by the authors. Licensee MDPI, Basel, Switzerland. This article is an open access article distributed under the terms and conditions of the Creative Commons Attribution (CC BY) license (<https://creativecommons.org/licenses/by/4.0/>).

1. Introduction

The consumption and demand for nickel increased in line with the production of stainless steel, nickel-based superalloys, and the raw material for Li-ion batteries. Policy changes in many countries to reduce greenhouse gas emissions, one of which is the conversion of internal combustion engine vehicles to electric vehicles (EV). The rise in EV production increases the nickel extraction from laterite nickel ore to meet the demand for class 1 nickel as raw material for EV batteries. Laterite nickel ore can be classified into saprolite and limonite types. In 2021, most of the nickel production emanated from saprolite type of laterite nickel ore which was processed via pyrometallurgical route mainly using rotary kiln–electric furnace (RKEF) technology to produce class 2 nickel such as ferronickel and nickel pig iron. The processing of limonite-type laterite nickel ore is still challenging both in terms of technology and the leach residue (tailings) produced, which require special attention for handling. High-pressure acid leach (HPAL) is one of the considered technologies for processing limonite type of laterite nickel ore. The HPAL technology was applied at Ravensthorpe in Australia, Meta Nickel and Goerdes in Turkey, Murrin

Murrin in Australia, Goro in New Caledonia, Ambatovy in Madagascar, Ramu in Papua New Guinea, Taganito and Coral Bay in the Philippines, and currently, Halmahera Persada Lygend in Indonesia [1–3]. In those projects, the leach residue is either placed in the tailings dam, as in the case of Taganito [4], dried by filter press and stacked, as in the case of Halmahera Persada Lygend, or placed in the deep sea, as in the case of Ramu [5]. However, the leakage of the pipeline for deep sea tailing placement was reported at Ramu, which forced a different treatment method for HPAL tailing, e.g., to extract iron and chromium [5].

An alternative technology is now being developed to process the laterite nickel ore by combining pyrometallurgy and hydrometallurgy. The nickel ore and sulfuric acid mixture is roasted in a rotary kiln at a specific temperature range. The roasted nickel ore is leached by water or weak sulfuric acid in a tank to dissolve nickel sulfate into a solution. The natrojarosite residue is produced during the iron and aluminum separation step. The amount of natrojarosite is around 20% of the processed laterite nickel ore. In general, natrojarosite residue behaves similarly to HPAL residue, which requires specific pre-treatment, special handling, and careful storage.

The jarosite is also produced from the zinc processing plant during iron precipitation, where each ton of zinc produced generates around 0.5 tons of jarosite as waste. Therefore, the utilization of jarosite has become a concern of researchers worldwide. Jarosite as a partial replacement for cement has been reported by Ray et al., where the increase of jarosite up to 15% improved the mechanical properties of cement [6]. Ahamed et al. [7] investigated the production of Zn-Fe alloys from jarosite by hydrometallurgy and electrometallurgy routes. The recovery of valuable metals from jarosite by pyrometallurgy route was also reported extensively, especially for iron extraction [8–11].

This study aims to utilize the natrojarosite residue from laterite nickel ore processing by sulfuric acid leaching as a secondary source of raw materials for producing iron and sulfuric acid. Due to the high sulfur content in the natrojarosite residue, which negatively affects the steel products, the sulfur separation shall be carried out, e.g., by roasting. The released sulfur in the form of sulfur dioxide, in principle, can be sent back to the sulfuric acid plant, which is then reused in the nickel processing plant. This sustainable utilization of natrojarosite residue as a source of iron and sulfur can reduce the environmental impacts related to mining activities for iron and sulfur, waste management, and energy needs.

2. Materials and Methods

2.1. Materials

The natrojarosite residue originated from a nickel extraction processing pilot plant in West Java, Indonesia. The sample was dried in an oven at 150 °C for 10 h to remove the surface moisture. The size reduction process was performed using a roll crusher and a ball mill to obtain a grain size of less than 65# (−0.210 mm). Coconut shell charcoal was used as a reductant, which was prepared by grinding using a ball mill to obtain a size of less than 60# (−0.250 mm). The mineralogical composition of the natrojarosite residue based on X-ray diffraction (XRD) using a Rigaku SmartLab diffractometer and X-ray fluorescence (XRF) using a Rigaku Supermini 200 is shown in Table 1. The iron, sulfur, and calcium contents in the jarosite residue are 16.23%, 12.18%, and 9.06%, respectively. The proximate analysis of the coconut shell charcoal is listed in Table 2.

Table 1. Mineralogical composition of natrojarosite residue (in wt%).

$\text{NaFe}_3(\text{SO}_4)_2(\text{OH})_6$	$\text{CaSO}_4 \cdot 2\text{H}_2\text{O}$	Fe_2O_3	$\text{Al}_2(\text{SO}_4)_3 \cdot 12\text{H}_2\text{O}$	$\text{MgSO}_4 \cdot 2\text{H}_2\text{O}$	
8.71	38.91	18.89	10.68	4.09	
$\text{NiSO}_4 \cdot 6\text{H}_2\text{O}$	$\text{Cr}_2(\text{SO}_4)_3$	SiO_2	MnO_2	Moisture	Other
9.03	0.75	2.80	1.73	3.92	0.45

Table 2. Proximate analysis of coconut shell charcoal (in wt%) and its calorific value.

Moisture	Ash	Volatile Matter	Fixed Carbon	Total Sulfur	Gross Calorific Value (Kcal/kg)
7.01	1.95	16.57	74.47	0.02	6.987

2.2. Experimental Method

For the experiments of sulfur removal via roasting, 10 g of natrojarosite residue was inserted into a porcelain cup without a lid; placed into a muffle furnace; and then heated isothermally at different temperatures of 500, 600, 700, 800, 900, 1000, and 1100 °C for 4 h. Three replicate samples were roasted for each roasting temperature. Before and after roasting, the samples were weighed using an analytical balance to determine their weight losses. The chemical composition of the roasted samples was determined by XRF, and the phases formed in the roasted samples were analyzed by XRD. Furthermore, the thermogravimetric analysis (TG) and differential thermal analysis (DTA) of the natrojarosite were carried out using Setaram SE 1600. During the TG-DTA analysis, approximately 13 mg of natrojarosite sample was heated to 1200 °C in a nitrogen atmosphere at a heating rate of 10 °C/min. During the heating process, the mass change and calorimetric effect were recorded, and the thermogravimetric and differential thermal analysis curves were obtained.

For the experiments of iron extraction via reduction, two different types of feed were considered, i.e., unroasted (initial) natrojarosite residue and roasted natrojarosite residue at 1100 °C. These residues were molded into cylindrical briquettes each with an average weight of 3–4 g and a thickness of 10–15 mm using a steel die, which was then pressed with a compressive strength of 5 metric tons for 5 min. Before a briquette was placed in a 20 mL porcelain crucible, the bottom of the porcelain crucible was protected by placing a layer of 0.5 g alumina powder, followed by adding approximately 1 g of coconut shell charcoal to prevent direct contact between the briquette and the porcelain crucible and alumina powder. After a briquette was inserted into the crucible, approximately 3 g of coconut shell charcoal was added to cover the whole briquette surface, thus providing a sufficient reductant source for the iron oxide reduction. To prevent direct contact of the charcoal with the surrounding air, 2 g of alumina powder was added to the top layer of the charcoal. The crucibles were placed inside a muffle furnace in which a type B thermocouple was installed for temperature controlling and monitoring. The reduction experiments were performed at an isothermal temperature of 1000 °C for 2 h, at an isothermal temperature of 1200 °C for 2 h, and via an isothermal–temperature gradient pattern (ITGP) starting from 1000 °C to a final temperature of 1400 °C, with a heating rate of 8 °C/minute for a total heating duration of 2 h. The latter was tested to examine the possibility of producing iron granules, as observed in previous work [12–14].

An additional reduction experiment was performed to evaluate the effect of composing natrojarosite residue and coconut charcoal in the briquette on the iron reduction. Natrojarosite residue was mixed with coconut charcoal weighted 20% of the residue. The mixture was then formed into a briquette through a similar procedure mentioned before. The composite briquette was reduced via an isothermal–temperature gradient pattern (ITGP) with a heating pattern identical to that of a non-composite briquette.

After the reduction experiments, the reduced briquettes were naturally cooled and were prepared through a conventional metallographic preparation technique, i.e., the samples were mounted in resin and cross-sectioned through mechanical polishing. The microstructure of the samples was characterized by a scanning electron microscope (SEM, JEOL JSM 6510 A), and the chemical composition of the micro area was analyzed by an energy dispersive spectrometer (EDS) available within the SEM.

2.3. Thermodynamic Simulation Method

A thermodynamic simulation was performed using FactSage 8.0 [15] to evaluate the phase changes in the natrojarosite residue during heating. Natrojarosite residue of 100 g

with chemical composition as shown in Table 1 was used as the basis of the simulation. Various key databases were taken into account in the thermodynamic simulation, such as FactPS database for the pure element, stoichiometric compounds, and gas phase; FToxid database for oxide solid solutions and oxide liquid solutions; and FTmisc for sulfide and alloys. The type and amount of phases resulting from the equilibrium of natrojarosite residues from room temperature to 1400 °C were the output of this thermodynamic simulation.

3. Results and Discussion

3.1. Sulfur Removal

The appearance of the samples before and after roasting at 500–1100 °C for 4 h are provided in Figure 1. The color of the roasted samples changed from yellowish-brown on the initial sample to reddish-brown after roasting at 500–700 °C to dark brown after roasting at 800–1000 °C and further to black after roasting at 1100 °C. The color changes coincided with the minerals/phases change during the roasting, as shown in the XRD analysis results in Figure 2. The main phase of minerals in the initial sample was natrojarosite, calcium sulfate hydrate, aluminum sulfate hydrate, and magnesium sulfate hydrate. After being roasted at 500 to 800 °C, the anhydrite phase and hematite were revealed. At 900 to 1100 °C, the hematite transformed to maghemite. At 1100 °C, the anhydrite tended to disappear due to its dissociation into calcium oxide and sulfur dioxide, followed by reaction between calcium oxide, aluminum oxide, and silicon oxide forming $\text{Ca}_2\text{Al}_2\text{SiO}_7$.

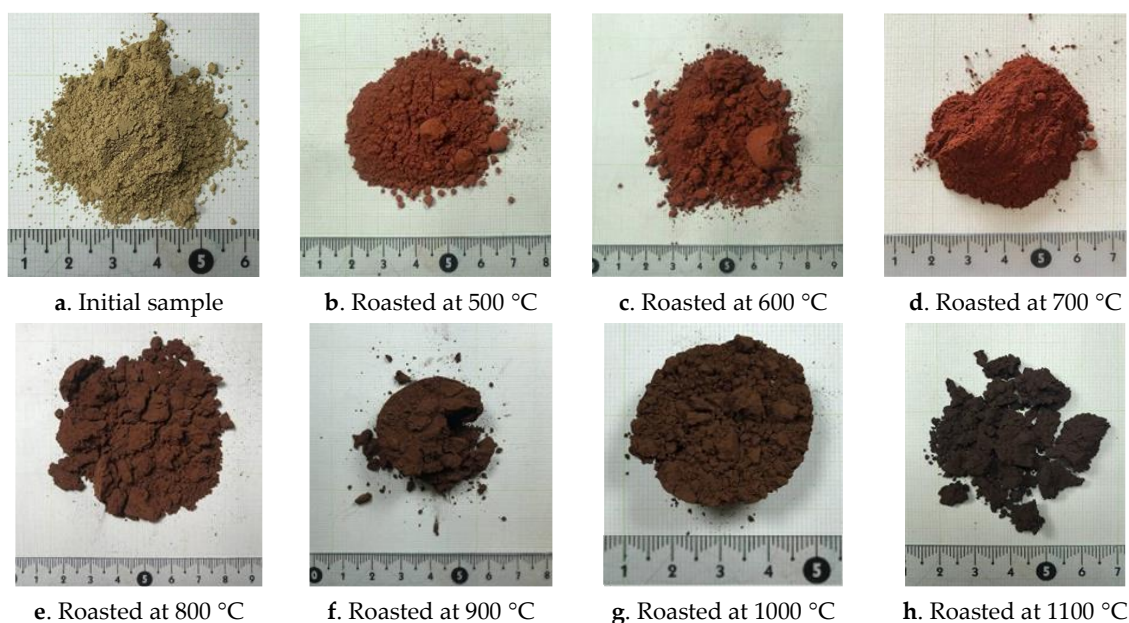


Figure 1. The physical appearance of the samples before and after roasting at different temperatures for 4 h.

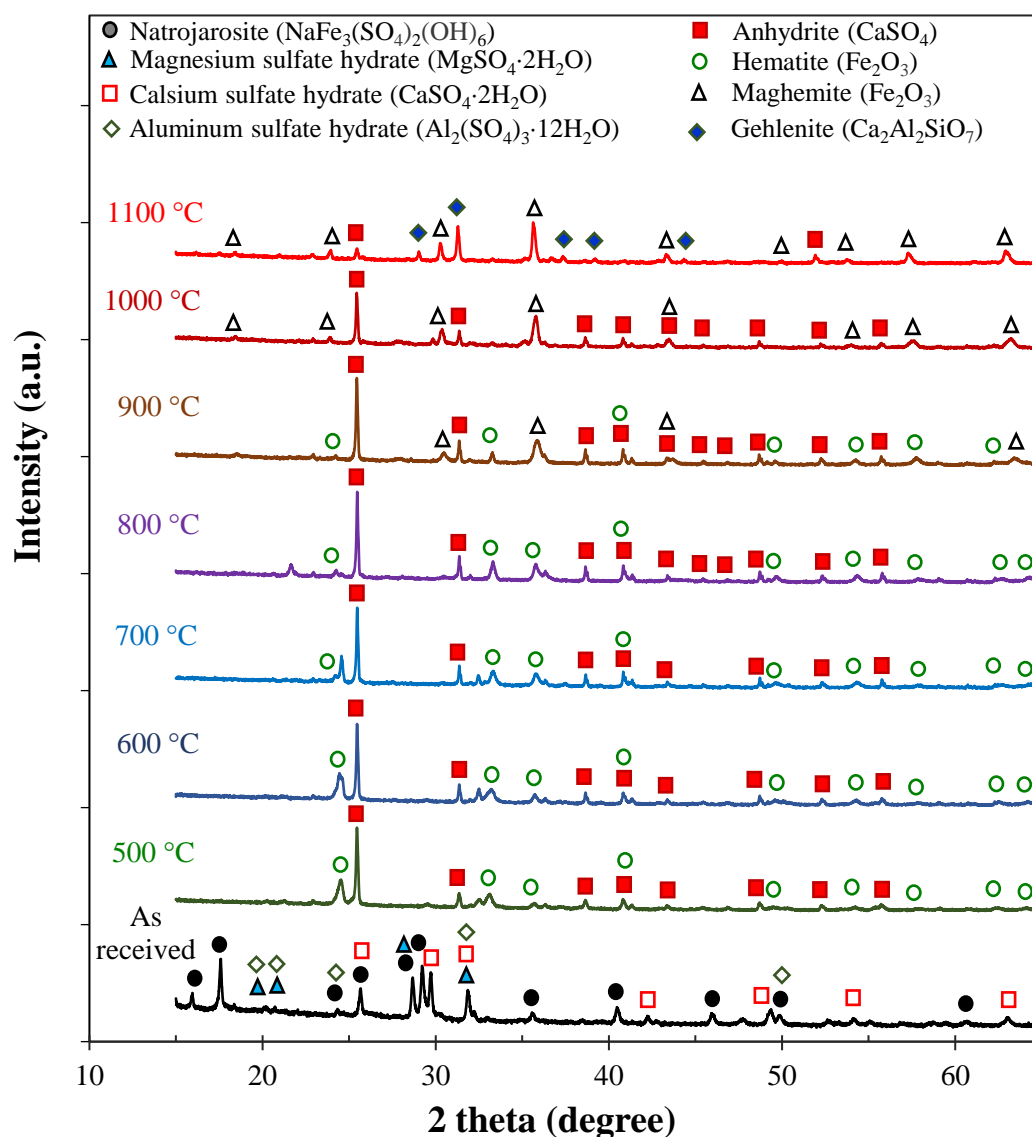
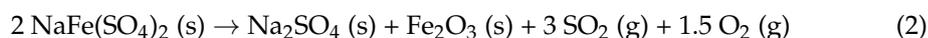
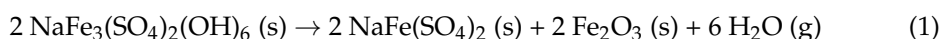


Figure 2. The results of XRD analysis on the initial and roasted samples at temperatures of 500–1100 °C.

The results of the thermodynamic simulation of high temperature treatment of natrojarosite residue using FactSage 8.0 are shown in Figure 3. The natrojarosite data are not available in the current version of thermochemical database; therefore, the sodium sulfate (Na_2SO_4) and ferric sulfate ($\text{Fe}_2(\text{SO}_4)_3$) are stable at room temperature instead of natrojarosite ($\text{NaFe}_3(\text{SO}_4)_2(\text{OH})_6$). Frost et al. [16] and Desborough et al. [17] reported that natrojarosite dissociated in two steps: namely, dihydroxylation at a temperature range of 215–352 °C and releasing sulfur dioxide (SO_2) gas at 555–595 °C according to the following equation:



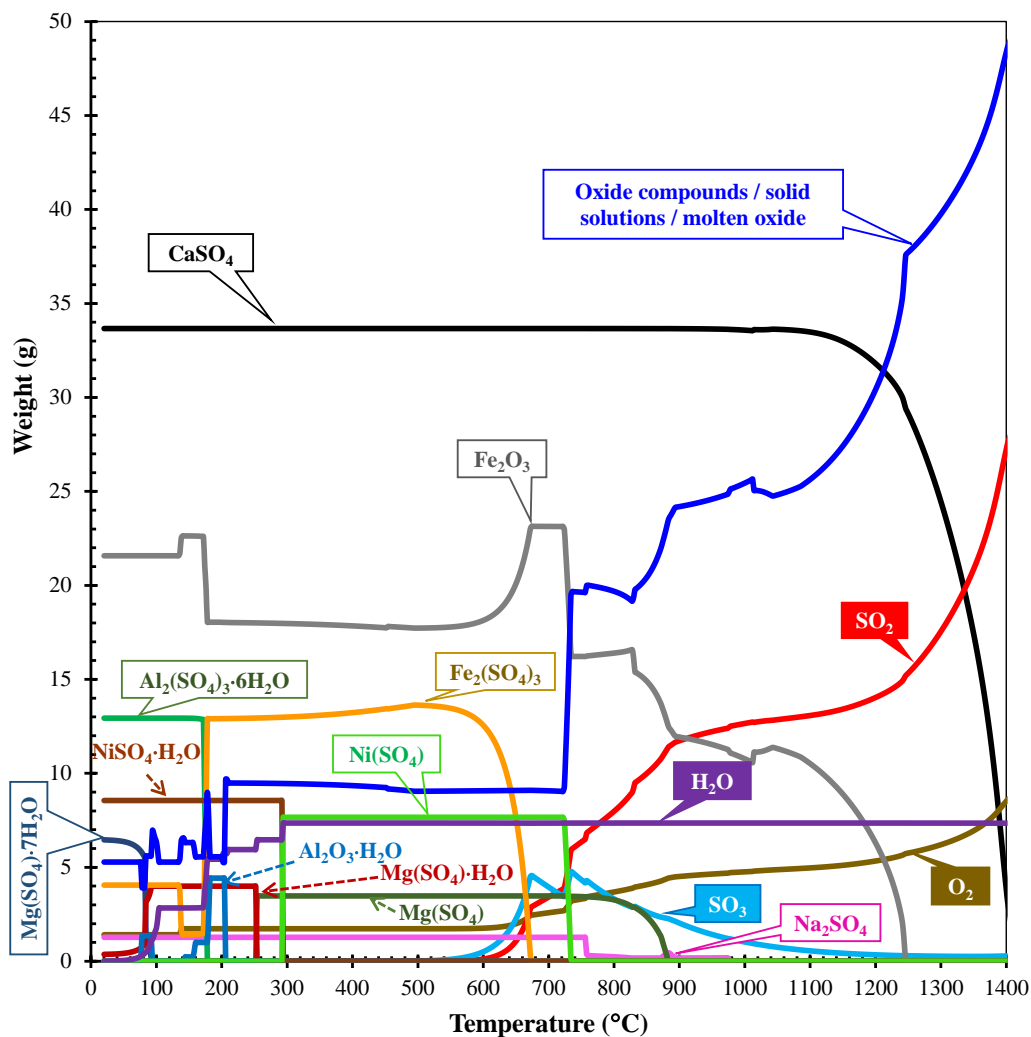


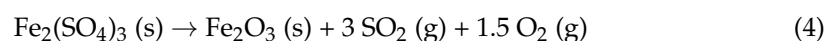
Figure 3. Thermochemical calculation by FactSage during the heating of 100 g of natrojarosite residue.

Based on the XRD results in Figure 2, the natrojarosite completely disappeared at a temperature of 500 °C and higher, which indicated that the dissociation of the natrojarosite occurred at a temperature of less than 500 °C. A similar result was reported by Zhu et al. [11], Kerolli-Mustafa et al. [18], and Linsong et al. [19], who observed that the dissociation of natrojarosite occurred at about 400 °C.

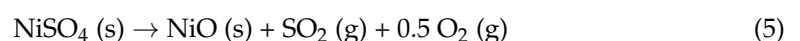
The thermochemical calculation results in Figure 3 show that at 180 °C aluminum sulfate hexahydrate transforms into alumina hydrate ($\text{Al}_2\text{O}_3 \cdot \text{H}_2\text{O}$) by releasing sulfur dioxide (SO_2), moisture (H_2O), and oxygen (O_2), according to Equation (3).

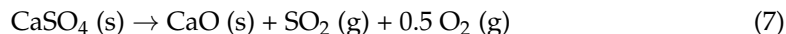
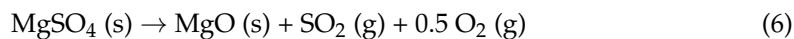


Ferric sulfate starts to dissociate into hematite and sulfur dioxide at 572 °C and its dissociation is completed at 680 °C, as shown by Equation (4).



Nickel sulfate, magnesium sulfate, and calcium sulfate start dissociating into magnesium oxide, nickel oxide, and calcium oxide by releasing sulfur dioxide and oxygen at a temperature of 724, 800, and 1150 °C, respectively, following Equations (5)–(7).





The resulting oxides react forming oxide compounds, oxide solid solutions, or molten oxide/slag, depending on the temperature (blue line in Figure 3).

The TG/DTA measurement results of natrojarosite residue are shown in Figure 4. The natrojarosite residue decreased in weight during the heating from room temperature to 1200 °C. The phase changes estimated from the thermochemical simulation were taken into consideration in the interpretation of the TG/DTA measurement results. The weight loss due to the evaporation of water and dehydration in the natrojarosite residue can be seen in the temperature range of 90–150 °C (points 1 and 2 in Figure 4). Point 3 in Figure 4 seems to indicate the dissociation of natrojarosite following Equation 1, which takes place in the temperature range 390–450 °C. The dissociation of nickel sulfate and sodium sulfate appears to occur at 700–750 °C, as marked by point 4 in Figure 4. Point 5 in Figure 4 appears to be the dissociation of magnesium sulfate at 870–955 °C. Finally, the calcium sulfate starts to dissociate at 1000 °C (point 6 in Figure 4) which was confirmed by XRD measurements at 1100 °C, where the calcium sulfate pattern tended to disappear (see Figure 2).

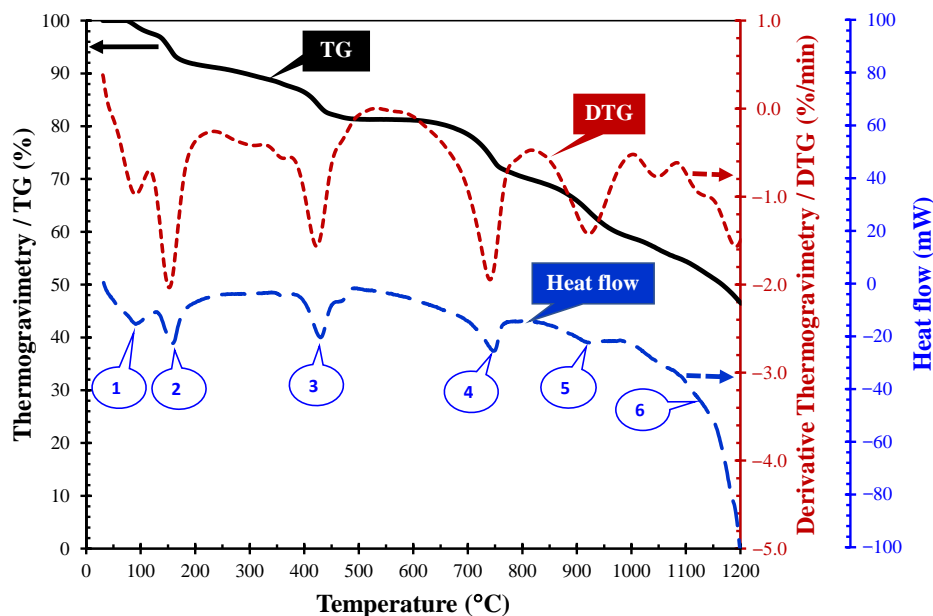


Figure 4. TG-DTA results for natrojarosite residues with a heating rate 10 °C/min.

Figure 5 shows the comparison of weight loss percentage between the roasting experiment, the results of the TG-DTA data, and the thermochemical calculation. All of the roasting experiment data, TG-DTA data, and thermochemical calculation showed an increase in weight loss of the sample with increasing temperature. The roasting experiment showed a weight loss of 17% at 500 °C, which then continued to increase until it reached 44.56% at 1100 °C. TG-DTA data showed a weight change similar to the roasting experiment. Changes in weight in every increase in temperature were caused by multi-stage decomposition that occurred in a certain temperature range. The deviation of thermochemical calculation compared to the roasting experiment and TG-TDA data, in particular at more than 300 °C, was due to the overestimation of the dissociation temperatures of ferric sulfate and calcium sulfate by the thermochemical software.

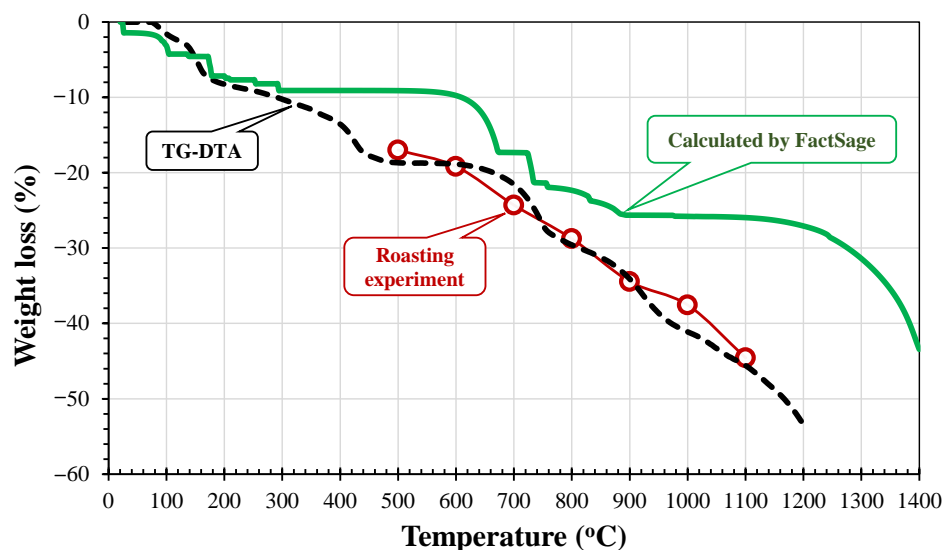


Figure 5. Weight losses versus temperature from roasting experiments, TG/DTA data, and thermochemical calculations by FactSage.

Changes in the chemical composition of the residue at different roasting temperatures were obtained from the XRF analysis, which was complemented with the estimated stable phases obtained from the XRD analysis and thermodynamic calculation. The data showed that the sulfur content decreased from 12.18% in the natrojarosite residue to 3.81% after roasting at 1100 °C as shown in Figure 6. Mombelli et al. [8] also reported that the sulfur content can be reduced from 8.86% in the jarosite to 2.55% in the jarosite after calcination at 1000 °C due to the release of sulfur in the form of SO_x gas. Mombelli et al. [8] and Zhu et al. [11] suggested that the resulting SO_x gas can be used for sulfuric acid production.

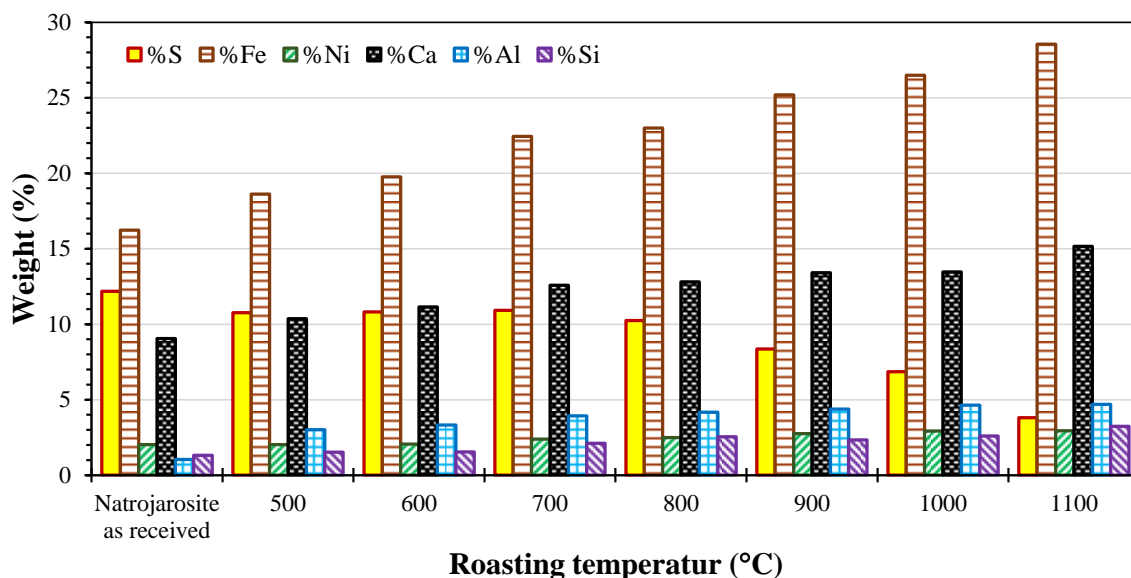


Figure 6. Changes in the contents of sulfur, iron, nickel, calcium, aluminum, and silicon after roasting at a temperature of 500–1100 °C.

In line with the removal of sulfur, the iron content in the jarosite residue increased from 16.23% to 28.54% and nickel content increased from 2.02% to 2.94% after being roasted at 1100 °C. Similar results were observed for calcium in which its content increased from 9.06% to 15.16%. The sulfur content can be further reduced by increasing the roasting temperature, as indicated by TG/DTA results in Figure 4.

The sulfur removal efficiency calculated from the roasting experiment results compared with the thermochemical calculation is shown in Figure 7. Based on the roasting experiment, the sulfur removal had already occurred at 500 °C, while the thermochemical calculation indicated that sulfur removal begins to occur at 570 °C. As it has been stated earlier, this discrepancy was due to the overestimation of ferric sulfate and calcium sulfate dissociation temperatures in the thermochemical calculation. The roasting experiment data shows that the sulfur removal efficiency increased from 26% at 500 °C to 82% at 1100 °C.

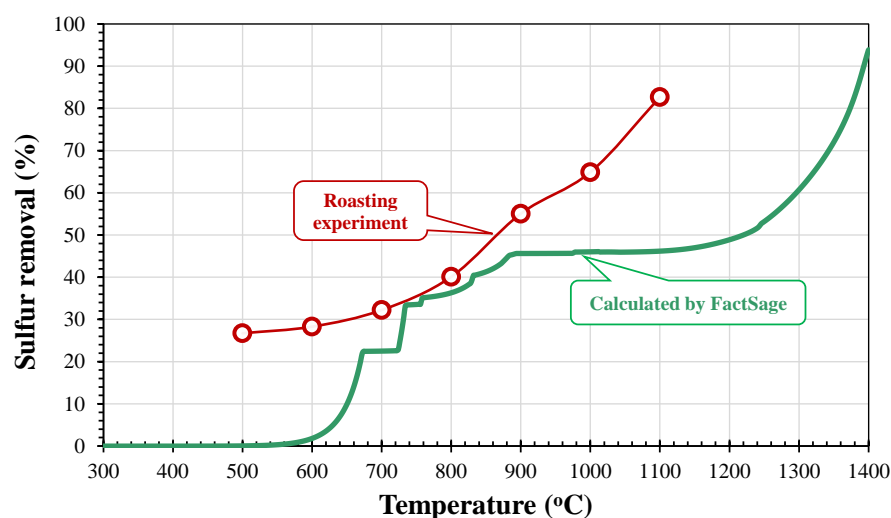


Figure 7. Comparison of sulfur removal efficiency between the roasting experiment and thermochemical calculation.

3.2. Extraction of Iron from the Unroasted Natrojarosite

The SEM images of reduced briquettes of unroasted (initial) natrojarosite residue are shown in Figure 8. The chemical composition based on EDS detection for each area or each point on the SEM images in Figure 8 is presented in Figure 9. The carbon content was not included in the EDS analysis due to its low accuracy. At 1000 °C, the metallic iron was not formed which was confirmed by the high oxygen content in the reduced briquette of 40–42% as shown by points or areas 1 to 5 in Figures 8a and 9a. The sulfur content was in the range of 2–20%, indicating that the sulfur removal was not taken place adequately. At 1200 °C, metallic iron was formed in the reduced briquette of unroasted natrojarosite residue as shown in area 6 in Figure 8b, where the iron and sulfur contents were 98.37% and 0.17%, respectively. The inclusion in the form of iron sulfide (FeS) was detected in the reduced briquette at point 8 in Figure 8b. The oxide phases are shown at points and areas 9–11 in Figure 8b, where the iron content in areas 10 and 11 were 2.64 and 0.22%, respectively. The phosphorous content in the metal phase was maximum of 0.05%.

The isothermal-temperature gradient pattern (ITGP) from 1000–1400 °C was previously reported successful in separating metal in the form of nuggets or granules from limonite nickel ore [12] and iron sand concentrate (titanomagnetite) [13,14]. Unfortunately, no metal nugget or granule was produced in the case of natrojarosite residue. However, metallic iron was detected, as shown in area 13 in Figure 8c. Metallic iron contained 0.81% sulfur, 12.7% nickel, and 4.8% silicon. The final temperature of 1400 °C on the ITGP allowed the reduction of silicon oxide into silicon metal. The sulfur and iron content in the oxide phase were between 1–15% and 4–48%, respectively.

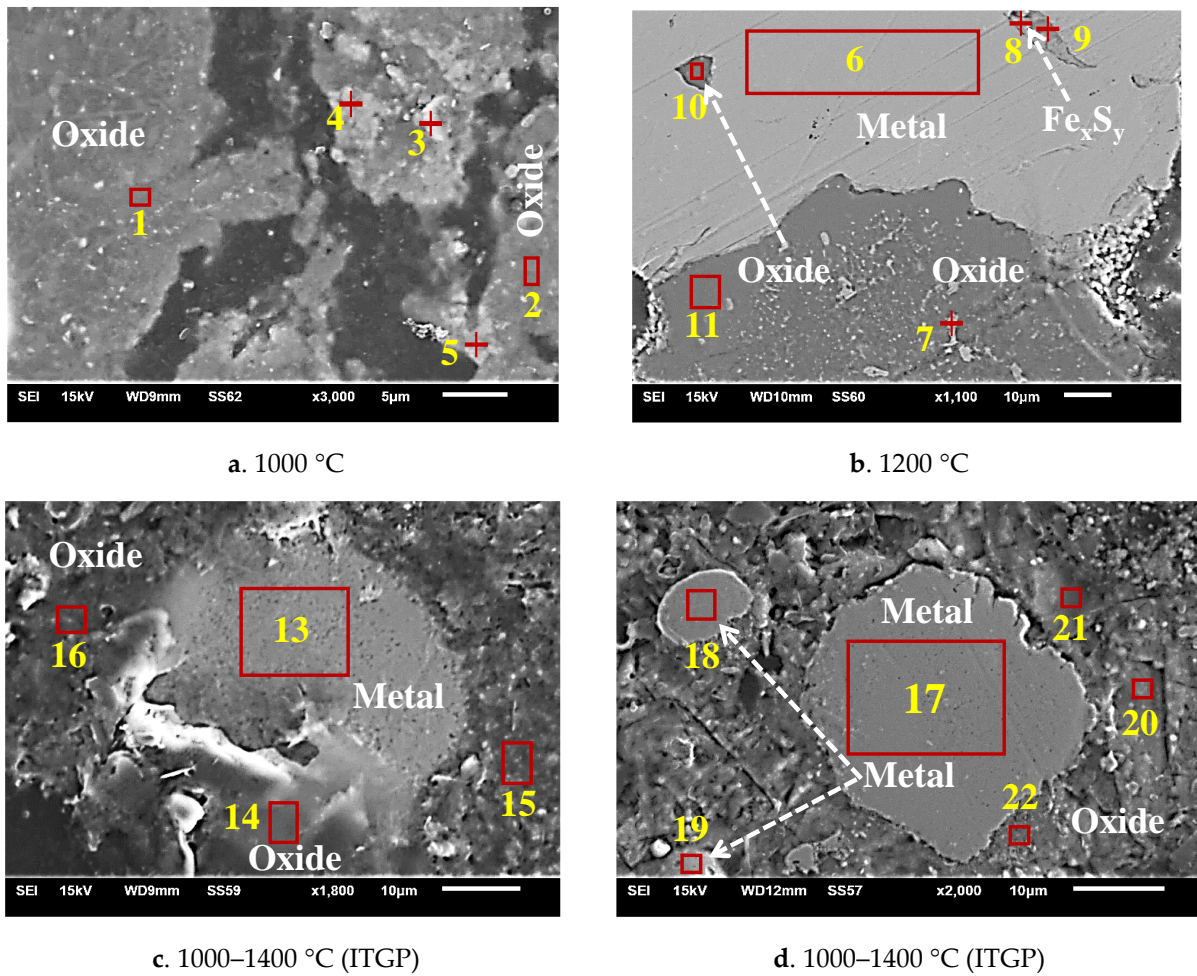


Figure 8. SEM images of unroasted natrojarosite residue after carbothermic reduction at different temperatures; ITGP = isothermal temperature gradient profile.

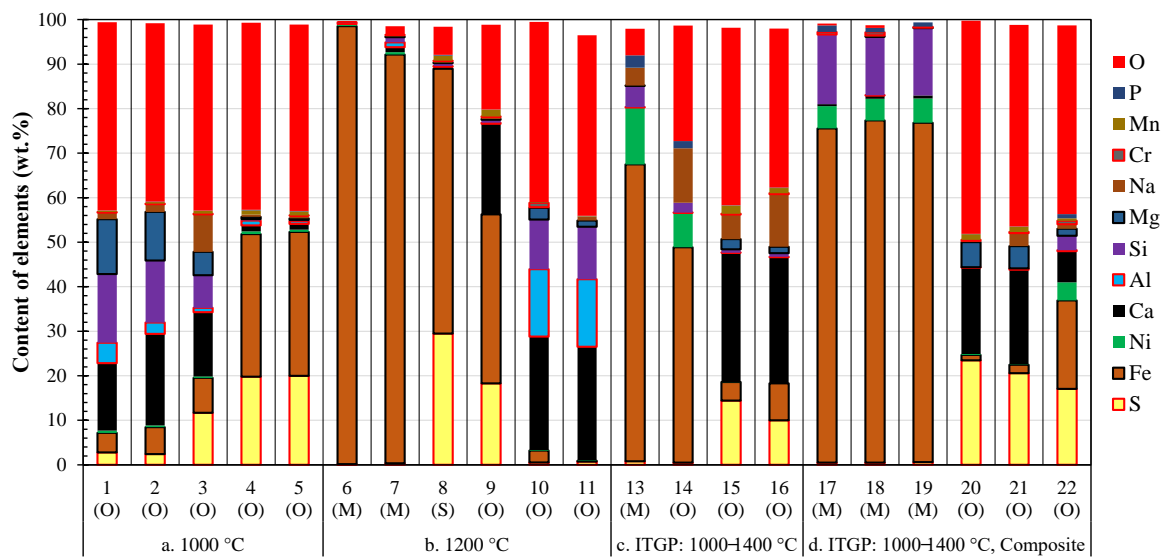


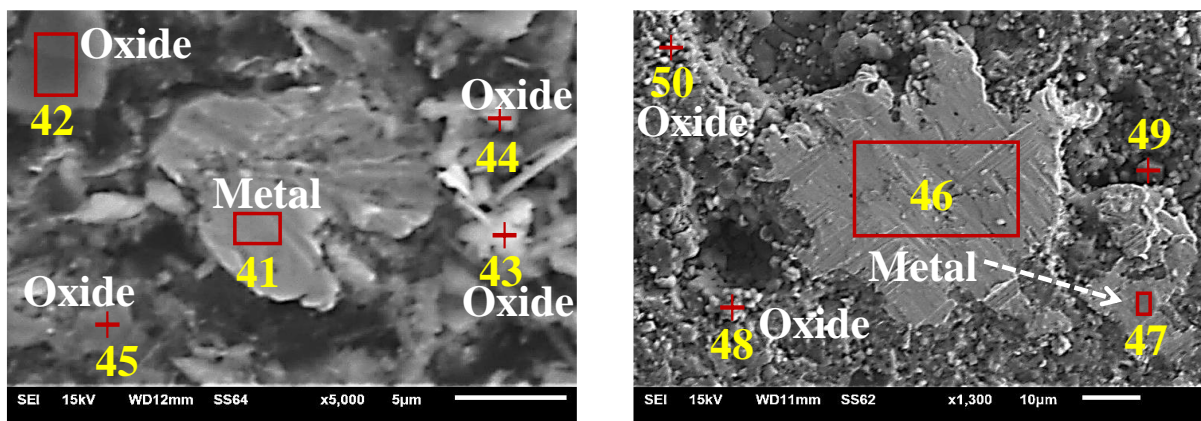
Figure 9. EDS analysis of unroasted natrojarosite residue after carbothermic reduction at different temperatures; ITGP = isothermal temperature gradient pattern. Numbers 1–22 refer to the location in Figure 8, O = oxide, M = metal, S = sulfide.

For reduced composite briquettes under ITGP, as shown in Figures 8d and 9d, the trend was similar to the non-composite briquettes, as shown in Figures 8c and 9c, in terms of the metallic iron formation. The sulfur, nickel, and silicon contents in the metal were 0.54%, 5.1%, and 14.6%, respectively. The iron content in the oxide phase was 1–19%. However, the sulfur content in the oxide phase of the reduced composite briquette was 17–24%, which was higher than in the non-composite briquette. This result was in line with the results of Zhang et al. [20], who used carbon to prevent the volatilization of sulfur in SO_x gas. As the amount of carbon increased, the degree of sulfidation also increased [20,21]. The optimum temperature for the degree of sulfidation was 800 °C. As the roasting temperature increased, the sulfidation degree tended to decrease [20,21].

As can be identified from Figure 9, in general, the sulfur content in the metal phases is less than in the oxide phase, which allows the separation of low-sulfur metallic iron from the high-sulfur oxide phase by crushing and magnetic separation. Lei et al. [5] reported the metallic iron separation from laterite sulfuric acid residue containing 3.71% sulfur and 44.62% iron by reduction roasting in the temperature range of 800–1400 °C. The metallic iron was recovered by magnetic separation in the form of metal concentrate. Lei et al. [5] showed that the sulfur content in the metal concentrate decreased from 3.66% at a reduction roasting temperature of 800 °C to 0.65% at 1400 °C.

3.3. Extraction of Iron from the Roasted Natrojarosite

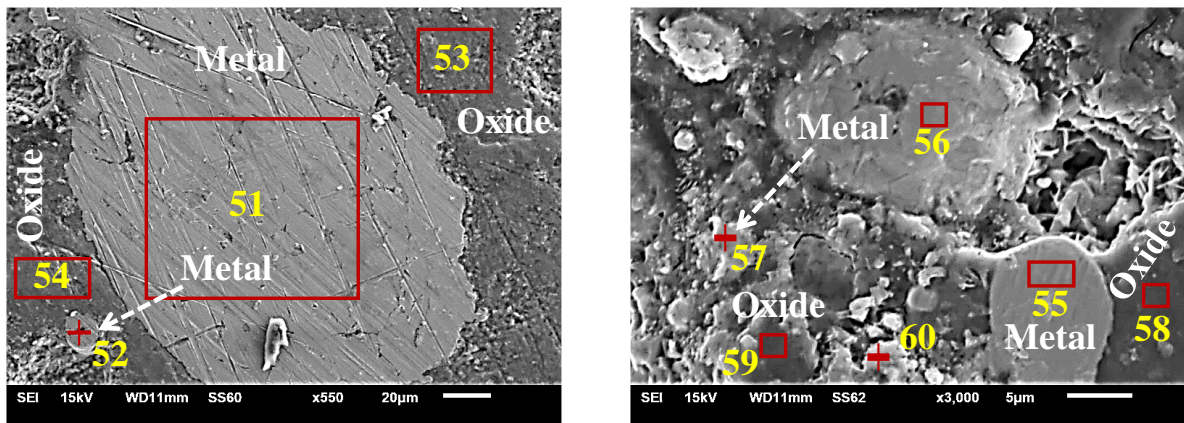
The natrojarosite residue that was roasted at 1100 °C for 4 h showed a decrease in sulfur content to 3.81% and an increase in iron content to 28.54%, as is shown in Figure 6. The results of the observations of the reduced briquettes of the roasted natrojarosite residue that were analyzed using SEM are presented in Figure 10, and the analysis of each point or each area by EDS is shown in Figure 11. For the briquette reduced at 1000 °C, the metallic iron was formed, as shown in area 41 in Figures 10a and 11a, where the iron, sulfur, and nickel contents were 83.83%, 1.00%, and 9%, respectively. The sulfur content in the oxide phase was in the range of 7–22%. The phosphorous content in the metal phase was a maximum of 0.08%.



a. 1000 °C

b. 1200 °C

Figure 10. Cont.



c. 1000–1400 °C (ITGP)

d. 1000–1400 °C (ITGP), composite

Figure 10. SEM images of roasted natrojarosite residue after carbothermic reduction at different temperatures; ITGP = isothermal temperature gradient profile.

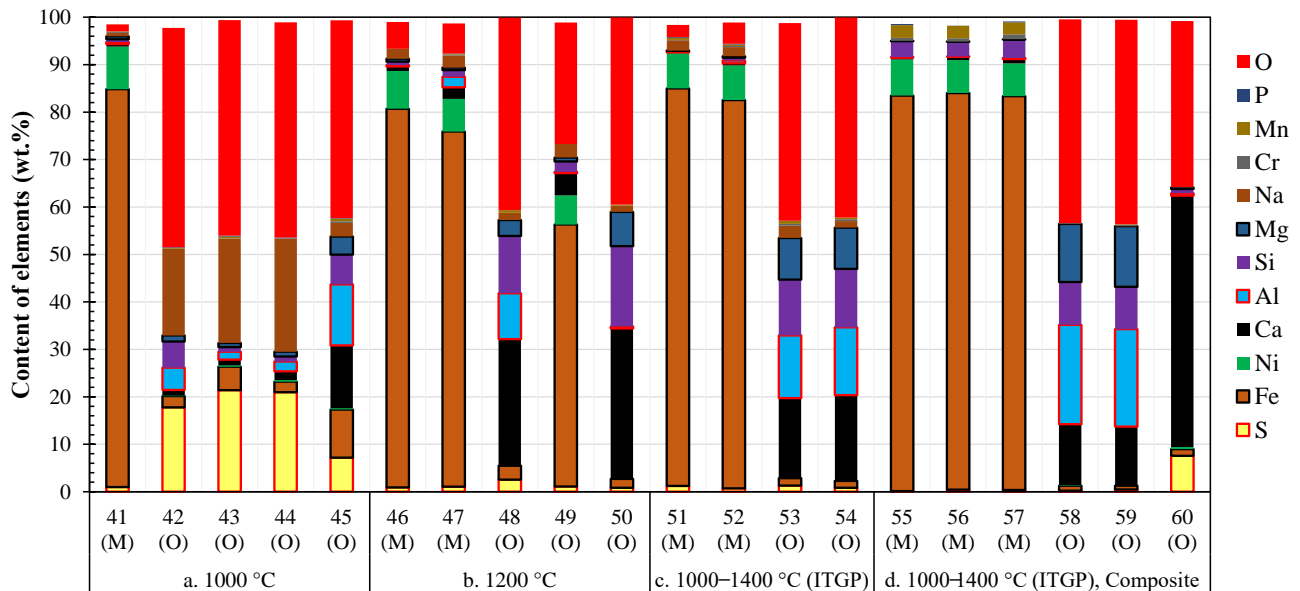


Figure 11. EDS analysis of roasted natrojarosite briquettes after carbothermic reduction at different temperatures; IGTP = isothermal gradient temperature profile. Numbers 41–60 refer to the location in Figure 10.

At 1200 °C, the metallic iron in the reduced briquette was formed with a sulfur content of 0.89% to 1.11% (Figures 10b and 11b). The sulfur content in the oxide phase was 0.8–2.5% which was less compared to the unroasted natrojarosite residue in Figures 8b and 9b. Similar to unroasted natrojarosite residue, the IGTP did not produce any iron granule separated from the slag. The metallic iron with a sulfur content of 0.7–1.2% was formed. The sulfur content in the slag was in the range of 0.8%–1.3% which was less compared to the unroasted natrojarosite residue.

Based on the present experimental results, it is suggested to remove sulfur and extract iron simultaneously in one stage where the initial natrojarosite residue is formed into a briquette which is immersed in a carbon-reducing agent and heated at 1200 °C. The optimum temperature of 1200 °C was also suggested by Lei et al. [5] who have conducted reduction roasting of acid leaching residue for extraction of metallic iron in the form of iron concentrate with iron and sulfur contents of 87% and 0.7%, respectively.

4. Conclusions

Natrojarosite residue is produced as a by-product of a nickel laterite processing by sulfuric acid leaching which needs to be handled and treated carefully. The natrojarosite residue can be utilized as raw material for iron production provided that the sulfur content meets the required level. The removal of sulfur from natrojarosite residue by roasting has been conducted in laboratory-scale experiments. The results show that a sulfur content of 12.18% in the unroasted natrojarosite residue can be reduced to 3.81% after roasting at 1100 °C for 4 h. The unroasted and roasted natrojarosite residues were then reduced by coconut shell charcoal in the temperature range of 1000–1400 °C. The results showed that the metallic iron could be obtained from both unroasted and roasted natrojarosite residue at a temperature of 1200 °C and higher. The sulfur content in the oxide phase of unroasted natrojarosite residue is significantly higher than roasted natrojarosite residue. However, the sulfur content in the metal phase was less than 0.9% from unroasted and less than 1.2% from roasted natrojarosite residue. These results indicated that the removal of sulfur and metal oxide reduction in the natrojarosite residue could be carried out simultaneously in one stage where the natrojarosite residue is reduced by carbonaceous material at a temperature of 1200 °C or higher.

Author Contributions: Conceptualization, Z.Z. and Z.A.; methodology, Z.A., Z.Z. and T.H.; software, Z.Z. and Z.A.; validation, Z.Z. and T.H.; formal analysis, Z.A. and Z.Z.; investigation, Z.A., M.M., J.D.C. and A.D.S.; data curation, Z.A., M.M., J.D.C., A.D.S. and Z.Z.; writing—original draft preparation, Z.A. and Z.Z.; writing—review and editing, Z.Z. and T.H.; supervision, Z.Z. and T.H.; funding acquisition, Z.Z., T.H. and A.H.Y. All authors have read and agreed to the published version of the manuscript.

Funding: This research was funded by the Ministry of Education, Culture, Research, and Technology of the Republic of Indonesia in 2022 (No. 083/E5/PG.02.00.PT/2022).

Institutional Review Board Statement: Not applicable.

Informed Consent Statement: Not applicable.

Data Availability Statement: Data is contained within the article.

Acknowledgments: The authors would like to thank PT. HMI (Hydrotech Metal Indonesia) and PT. Asco Prima Surya who have provided natrojarosite residue and coconut shell charcoal for the research materials.

Conflicts of Interest: The authors declare no conflict of interest.

References

1. Gabb, J. HPAL: Upping the pressure. *Glob. Min. Res.* **2018**. Available online: <https://gigametals.com/site/assets/files/4861/2018-03-19-hpal.pdf> (accessed on 15 June 2022).
2. Stanković, S.; Stopić, S.; Sokić, M.; Marković, B.; Friedrich, B. Review of the past, present, and future of the hydrometallurgical production of nickel and cobalt from lateritic ores. *Metall. Mater. Eng.* **2020**, *26*, 199–208. [[CrossRef](#)] [[PubMed](#)]
3. Gultom, T.; Sianipar, A. High pressure acid leaching: A newly introduced technology in Indonesia. *IOP Conf. Ser.* **2020**. Available online: <https://iopscience.iop.org/article/10.1088/1755-1315/413/1/012015> (accessed on 15 June 2022). [[CrossRef](#)]
4. Shibayama, K.; Yokogawa, T.; Sato, H.; Enomoto, M.; Nakai, O.; Ito, T.; Mizuno, F.; Hattori, Y. Taganito HPAL plant project. *Miner. Eng.* **2016**, *88*, 61–65. [[CrossRef](#)]
5. Lei, M.; Ma, B.; Chen, Y.; Liu, W.; Liu, B.; Lv, D.; Zhang, W.; Wang, C. Effective separation and beneficiation of iron and chromium from laterite sulfuric acid leach residue. *ACS Sustain. Chem. Eng.* **2020**, *8*, 3959–3968. [[CrossRef](#)]
6. Ray, S.; Daudi, L.; Yadav, H.; Ransinchung, G.D. Utilization of jarosite waste for the development of sustainable concrete by reducing the cement content. *J. Cleaner Prod.* **2020**, *272*, 122546. [[CrossRef](#)]
7. Ahamed, A.M.; Pons, M.N.; Ricoux, S.; Issa, S.; Goettmann, F.; Lapicque, F. New pathway for utilization of jarosite, an industrial waste of zinc hydrometallurgy. *Miner. Eng.* **2021**, *170*, 107030. [[CrossRef](#)]
8. Mombelli, D.; Mapelli, C.; Di Cecca, C.; Barella, S.; Gruttadauria, A.; Ragona, M.; Pisu, M.; Viola, A. Characterization of cast iron and slag produced by jarosite sludges reduction via Arc Transferred Plasma (ATP) reactor. *J. Environ. Chem. Eng.* **2018**, *6*, 773–783. [[CrossRef](#)]
9. Mombelli, D.; Mapelli, C.; Barella, S.; Gruttadauria, A.; Spada, E. Jarosite wastes reduction through blast furnace sludges for cast iron production. *J. Environ. Chem. Eng.* **2019**, *7*, 102966. [[CrossRef](#)]

10. Mombelli, D.; Gonçalves, D.L.; Mapelli, C.; Barella, S.; Gruttadauria, A. Processing and characterization of self-reducing briquettes made of jarosite and blast furnace sludges. *J. Sustain. Metall.* **2021**, *7*, 1603–1626. [[CrossRef](#)]
11. Zhu, D.; Yang, C.; Pan, J.; Guo, Z.; Li, S. New pyrometallurgical route for separation and recovery of Fe, Zn, In, Ga and S from jarosite residues. *J. Cleaner Prod.* **2018**, *205*, 781–788. [[CrossRef](#)]
12. Zulhan, Z.; Gibranata, I. Direct reduction of low grade nickel laterite ore to produce ferronickel using isothermal—Temperature gradient. *AIP Conf. Proc.* **2017**, *1805*, 040003. [[CrossRef](#)]
13. Zulhan, Z.; Lo, F. Iron nugget formation from iron sand/coal composite pellets under isothermal-temperature gradient profiles. *Ironmak. Steelmak.* **2021**, *48*, 1022–1029. [[CrossRef](#)]
14. Zulhan, Z.; Sutandar, C.L.; Suryani, I.; Basuki, E.A. Effect of temperature patterns on iron nugget formation in fluxless processing of titanomagnetite. *Sci. Rep.* **2022**, *12*, 8941. [[CrossRef](#)]
15. Bale, C.W.; Bélisle, E.; Chartrand, P.; Decterov, S.A.; Eriksson, G.; Gheribi, A.E.; Hack, K.; Jung, I.H.; Kang, Y.B.; Melançon, J.; et al. FactSage thermochemical software and databases—2010–2016. *Calphad* **2016**, *54*, 35–53. [[CrossRef](#)]
16. Frost, R.L.; Weier, M.L.; Martens, W. Thermal decomposition of jarosites of potassium, sodium and lead. *J. Therm. Anal. Calorim.* **2005**, *82*, 115–118. [[CrossRef](#)]
17. Desborough, G.A.; Smith, K.S.; Lowers, H.A.; Swayze, G.A.; Hammarstrom, J.M.; Diehl, S.F.; Leinz, R.W.; Driscoll, R.L. Mineralogical and chemical characteristics of some natural jarosites. *Geochim. Cosmochim. Acta.* **2010**, *74*, 1041–1056. [[CrossRef](#)]
18. Kerolli-Mustafa, M.; Mandic, V.; Curkovic, L.; Sipusic, J. Investigation of thermal decomposition of jarosite tailing waste: A prerequisite for comprehensive jarosite reuse and waste minimization. *J. Therm. Anal. Calorim.* **2016**, *123*, 421–430. [[CrossRef](#)]
19. Linsong, W.; Peng, Z.; Yu, F.; Sujun, L.; Yue, Y.; Li, W.; Wei, S. Recovery of metals from jarosite of hydrometallurgical nickel production by thermal treatment and leaching. *Hydrometallurgy* **2020**, *198*, 105493. [[CrossRef](#)]
20. Zhang, B.; Zhu, L.; Liu, W.; Han, J.; Jiao, F.; Qin, W. Sulfidation and sulfur fixation of jarosite residues during reduction roasting. *Metall. Mater. Trans. B* **2019**, *50*, 761–771. [[CrossRef](#)]
21. Wang, Y.; Yang, H.; Zhang, G.; Kang, J.; Wang, C. Comprehensive recovery and recycle of jarosite residues from zinc hydrometallurgy. *Chem. Eng. J. Adv.* **2020**, *3*, 100023. [[CrossRef](#)]

Disclaimer/Publisher’s Note: The statements, opinions and data contained in all publications are solely those of the individual author(s) and contributor(s) and not of MDPI and/or the editor(s). MDPI and/or the editor(s) disclaim responsibility for any injury to people or property resulting from any ideas, methods, instructions or products referred to in the content.